Modeling of Doubly Fed Induction Machine based Wind Turbines in ATP: challenges and experiences

G.R. Calzolari, C.R. Saldaña

Abstract— **In order to investigate the power system impact of wind turbines, it is essential to use accurate simulation models of wind turbines and power system. These models must correctly represent the electromagnetic and electromechanical behavior of the wind turbines in order to predict critical operational conditions and grid reinforcements. Power system elements such as busbars, lines, cables, etc. are built-in elements in the ATP (Alternative Transients Program). In contrast to this, wind turbines are not part of the tool. The main focus of the present work is to develop a comprehensive simulation model of the DFIG type wind turbine using ATP program. This paper presents the following issues related to the modeling carried out: a) a short explanation of the "Equivalent Wind Speed" model developed by Riso DTU b) a brief description of the DFIG type wind turbine basic components and an explanation of how each of them is modeled in ATP c) the maximum wind power extraction module written in TACS d) an initialization procedure of the complete model e) some ATP simulation results showing the DFIG behavior.**

Keywords: **Variable speed wind turbine, DFIG, ATP.**

I. INTRODUCTION

D UE to environmental concerns, the rising cost of fuel and the finiteness of fossil fuel reserves, there has been a strong penetration of renewal energy resources into the power supply network. Within renewable energy sources the wind energy is cost competitive, reliable and efficient. The main reasons that resulted in the fast development of wind power are: the immense potential of wind energy on the earth, the political and economic support from the governments and the development of wind turbine technology. Wind generation gradually becomes an important component of power generation in the grid due to the increasing number of wind power plants. Therefore, it is necessary to study the interaction between the wind turbines and the grid under steady state and transient conditions, especially in some critical situations like short-circuit fault, voltage dips, etc. Nowadays, Doubly Fed Induction Generator (DFIG) is most commonly used by the wind turbine industry for larger wind turbines. The most significant reason for this is the relatively small size of the power converter, approximately 30% of nominal turbine

G. Calzolari works in Projects and Studies, UTE, Paraguay 2431,Of 634, Montevideo 11800, Uruguay (e-mail of corresponding author: gcalzolari@ute.com.uy).
C. Saldaña works in Power System Protection, UTE, Bvar. A. Saravia 4292, Montevideo 11700, Uruguay (e-mail: gracclau@adinet.com.uy).

power, which is a cost efficient solution in order to obtain variable speed. Both active and reactive power can be controlled, so that the unity power factor can be maintained and it is even possible to use a variable speed wind generator as a source of reactive power. The increased number of wind farms based on DFIG brings a large amount of asynchronous generators in the power system, displacing conventional synchronous generators and reducing the system inertia. As the dynamics of asynchronous machines are different from those of synchronous machines, the grid could face technical challenges. In order to investigate the power system impact of wind turbines, it is essential to use accurate simulation models of wind turbines and power system. These models must correctly represent the electromagnetic and electromechanical behavior of the wind turbines in order to predict critical operational conditions and grid reinforcements. In order to develop a comprehensive DFIG type wind turbine model the ATP program is used as a tool.

II. WIND MODEL

Wind turbines convert the kinetic energy in the wind into mechanical energy. Therefore, a wind model in the form of time series is necessary in order to perform wind turbine simulations in a time domain. The wind speed is characterized by two main components: a) a mean wind speed profile over the rotor area, here considered as deterministic b) a turbulence which represents the stochastic variations of the wind speed around its mean value. The deterministic part of the wind is assumed constant in a ten-minute period. In this work the "Equivalent Wind Speed" model (EWS) developed by Riso DTU (National Laboratory for Sustainable Energy), Denmark, is chosen as a wind model [1],[2]. This model simulates the wind speed by an equivalent time series that reproduces the aerodynamic torque from a real wind turbine when applied to a specific aerodynamic model. The EWS model is an equivalent for the entire rotor that takes into account the stochastic and deterministic wind speed actions on the rotor area. The theoretical development of the EWS model is described in references [1],[2],[3].

Fig. 1 shows the block diagram of the EWS model implemented in TACS. The inputs of the model are: a) the mean wind speed at hub height b) three different white noises generated with Band-Limited White Noise block of Simulink MATLAB. The output of the model is the wind speed time series (v). The transfer functions, defined in [3] are:

$$H_{KAIMAL}(s) = \sqrt{\frac{4L_k\sigma^2}{2V_{hub}}} * \frac{0.0182c^2s^2 + 1.3653cs + 0.9846}{1.3463c^2s^2 + 3.7593cs + 1} \qquad (1)$$

where: $L_k = 8.1*\Lambda_1$ $\Lambda_1 = 0.7*H_{hub}$ if $H_{hub} < 30$m; $\Lambda_1 = 21$m

if $H_{hub} \geq 30m$; H_{hub} hub height [m]; V_{hub} mean speed at hub height [m/s]; σ turbulence standard deviation; $c = 4L_k/2\pi V_{hub}$
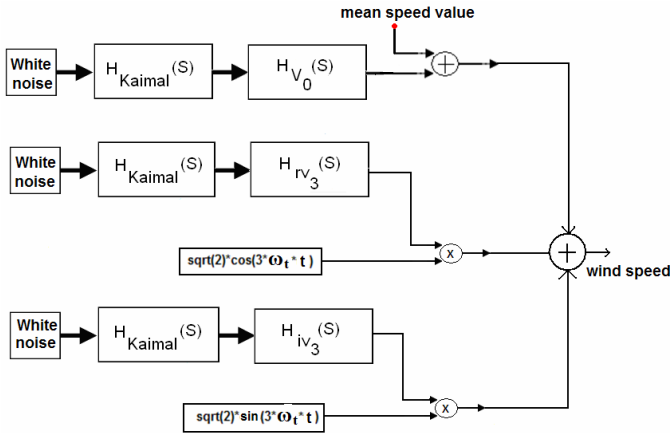

Fig. 1. EWS model in TACS

$$H_{vo}(s) = \frac{0.99 + 4.79ds}{1 + 7.35ds + 7.68d^2s^2} \quad (2)$$

$$H_{rv3}(s) = H_{iv3}(s) = \frac{0.0307 + 0.277ds}{1 + 1.77ds + 0.369d^2s^2} \quad (3)$$

where: $d = R/V_0$, R rotor radius

Fig. 1 shows that the EWS model is a function of the turbine angular speed (ω_t), therefore it can be applied to variable or constant rotor speed wind turbines models without additional modifications. Fig. 2 shows a time series of wind speed characterized by a mean speed of 18 m/s and turbulence intensity of 11.3%, resulting from an ATP simulation with time step equal to 50 ms.
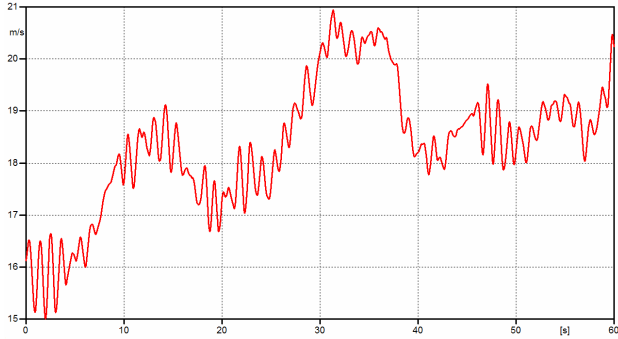

Fig. 2. Simulated time series of wind speed

III. DFIG WIND TURBINE COMPONENTS AND ATP MODELING

The typical DFIG configuration, illustrated in Fig. 3, consists of: a) a wind turbine b) a gearbox c) a wound rotor induction generator d) a bidirectional back-to-back power converter e) rotor and grid side converter controllers f) a power controller.

A. Aerodynamic model

The aerodynamic model evaluates the turbine torque (T_{aero}) as a function of wind speed (v), the turbine angular speed (ω_t) and the power coefficient (C_p) as indicated by (4).

$$T_{aero} = \frac{1}{2} * \rho * \pi * R^2 * v^3 * C_p(\lambda, \beta) * \frac{1}{\omega_t} \quad (4)$$
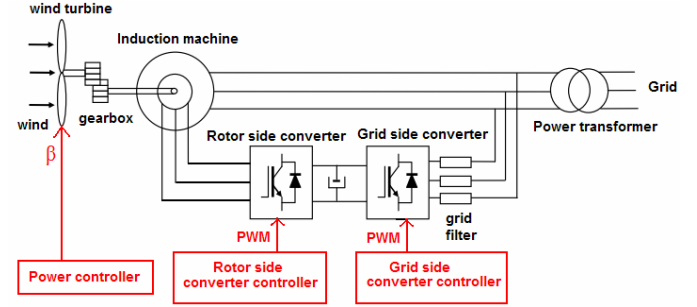

Fig. 3. Typical DFIG configuration

where: ρ air density, R radius of the turbine rotor, λ tip speed ratio, β pitch angle. In order to implement (4) in TACS, the following process is carried out: a) the output of the EWS model gives v b) the ω_t is accessed by means of the Type-92 TACS source component and referred to low speed side c) the power controller provides β d) the λ is calculated by dividing the speed of the tips of the turbine blades by the speed of the wind e) the calculation of C_p is carried out following the approach presented in [4] and is implemented in routine TACS using device Type-69.

B. Mechanical system model

The mechanical system is constituted by the three blades linked to the hub, coupled to the low speed shaft, which is linked to the gearbox, which in turn is connected to the high speed shaft coupled to the generator rotor. The gearbox converts the low speed in the turbine rotor into high speed in the generator rotor. The induction generator is modeled with "Universal Machine" of ATP [5],[6]. The mechanical system is represented through an equivalent electrical network with lumped R,L,C, elements and a single mass representation is chosen by the authors at this stage. The turbine torque given by (4) is added to the equivalent network as a current source (TYPE 60) by the user and the electromagnetic torque is also added as a current source by the ATP. All mechanical quantities (torques, moment of inertia and damping coefficient) are referred to the high speed side through the gearbox ratio.

C. Induction generator, power converters, grid filter

A wound rotor induction generator with the stator windings directly connected to the grid and with the rotor windings fed by a bidirectional back-to-back power converter that is also connected to the grid, is in charge of converting mechanical energy into electrical energy. As mentioned before it is modeled with Universal Machine (UM) of ATP.

Some scenarios are studied and the associated simulations start under steady state conditions and the "Automatic Initialization" method for the purpose of the UM steady state initialization is chosen.

The UM component allows both stator and rotor windings to be directly connected to the three-phase voltage-source converters, termed as Rotor Side Converter (RSC) and Grid Side Converter (GSC). Figure 4 shows the ATP implementation.
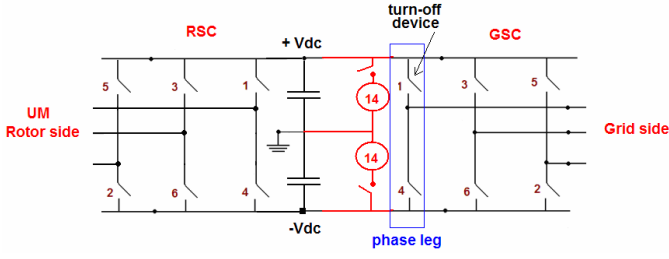
Fig. 4. RSC and GSC implementation in ATP

For controlling the AC voltage outputs of power converters the technique known as Pulse Width Modulation (PWM) is utilized for each converter. This varies the duty cycle of the turn-off devices at a high switching frequency to achieve three target low frequency output voltages [7]. The RSC controller generates three rotor frequency sinusoidal voltage references displaced in time by 120º. The GSC controller generates three power frequency sinusoidal voltage references displaced in time by 120º. The PWM process is a simple comparison between each of the reference waveforms and a sawtooth or a triangular carrier waveform. For example, let's consider the phase leg indicated in Fig. 4, when the reference waveform is greater than the carrier waveform, switch 1 closes and switch 4 opens, if not switch 1 opens and switch 4 closes. Each of the turn-off devices is modeled as a Type-13 simple TACS-controlled switch, whose OPEN/CLOSE signal is defined as a logical variable resulting from the comparison between the reference and sawtooth signals.

Between the two converters capacitors are placed in order to keep the voltage variations in the DC-link voltage small as shown in Fig. 4. For steady state initialization of the capacitors, two very low frequency Type 14 sources of 0.000001 Hz with amplitude +/- Vdc are added, and after the first 5 ms, they are removed.

The grid filter consists of an inductance L_f in series with a resistance R_f in order to reduce the harmonics in the currents caused by semiconductor switching.

D. Rotor and grid side converter controllers

The main task of the Rotor Side Converter Controller (RSCC) is to control the induction machine. This is done by transforming machine equations in phase quantities into dq0 quantities by using Park's transformation. The d-axis is aligned with the stator flux of the DFIG. With this reference frame, the following expressions could be derived for the electromagnetic torque (T_e) and the reactive power at the stator terminals (Q_s) [8]:

$$T_e = (-\frac{p\lambda_{ds}M}{Ll_s + M}) * i'_{qr} \tag{5}$$

$$Q_s = [\frac{V_{qs}}{Ll_s + M}] * (\lambda_{ds} - Mi'_{dr}) \tag{6}$$

where: p number of pole pairs, λ_{ds} d-axis stator flux, M magnetizing inductance, Ll_s stator leakage inductance, V_{qs} q-axis stator voltage, i'_{qr} and i'_{dr} q-d-axis rotor currents referred to the stator side. From (5) and (6) it can be observed that it is possible to control the electromagnetic torque by the q-axis rotor current and the power factor at the stator terminals by the

d-axis rotor current. The RSCC consists of two fast d-q-axis rotor current control loops, whose block diagrams are shown in Fig. 5. In this figure all the rotor magnitudes are referred to the stator side.
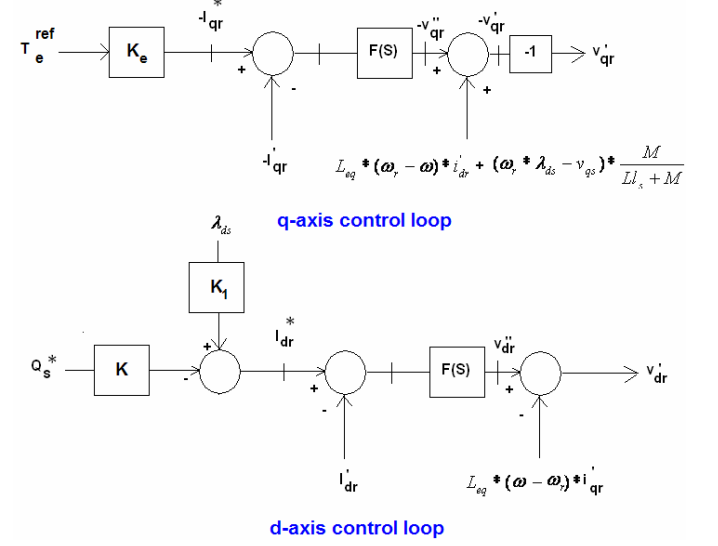

Fig. 5. Block diagrams of the RSCC controller

where: $K_e = \frac{Ll_s + M}{p\lambda_{ds}M}$ $K = \frac{Ll_s + M}{Mv_{qs}}$ $K_1 = \frac{1}{M}$

Inputs T_e^{ref} and Q_S^* are user defined reference values of the electromagnetic torque and the reactive power at the stator terminals. The reference currents i_{qr}^* and i_{dr}^* are derived from (5) and (6). The L_{eq} is an equivalent inductance defined by:

$$\frac{1}{L_{eq}} = \frac{Ll_s + M}{Ll_s * Ll'_r + M * Ll'_r + M * Ll_s} \tag{7}$$

where: Ll'_r rotor leakage inductance. Inputs ω and ω_r are the synchronous and generator rotor angular velocities.

The measured d-q-axis rotor currents i'_{dr}, i'_{qr} are compared with i_{dr}^* and i_{qr}^* respectively and the errors are reduced to zero by a PI regulator whose transfer function is given by:

$$F(s) = 0.2728 * (1 + \frac{1}{0.001795s}) \tag{8}$$

The Internal Model Control (IMC) method for designing the PI controller is chosen by the authors [9].

The outputs of the current controllers are the q-axis rotor voltage v'_{qr} and the d-axis rotor voltage v'_{dr}. From them and applying the inverse Park's transformation, three rotor frequency sinusoidal voltage references are obtained, as required by PWM technique.

The RSCC controller is implemented in TACS in the following way: a) the T_e^{ref} is given by the power controller and it will be described in ítem IV b) the Q_S^* comes from the user -defined scenarios c) the rotor currents and stator voltages in phase quantities are measured and passed to TACS by Type-90 and Type-91 sources. The Park's transformation is written in TACS and then dq0 values are derived d) the d-axis stator flux is calculated according to [10] and implemented in TACS e) the ω_r is accessed by means of the Type-92 TACS source component f) the inverse Park's transformation is also written in TACS g) the PI transfer function is represented by S-blocks.

The main objective of the Grid Side Converter Controller (GSCC) is to keep the DC-link voltage constant and control the reactive power exchange with the grid. This is done by transforming grid filter equations in phase quantities into dq0 quantities by using Park's transformation. The d-axis is aligned with the stator (or supply) voltage. The approach presented in [10] is followed by the authors in order to derive the control loops, whose block diagrams are shown in Fig. 6.
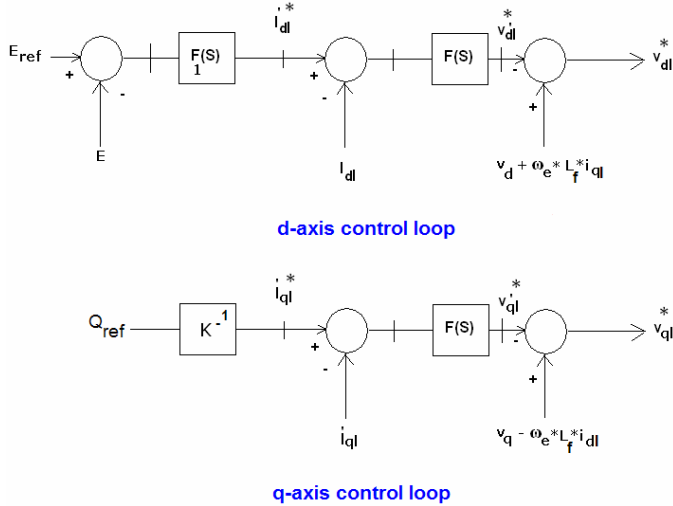

d-axis control loop

q-axis control loop

Fig. 6. Block diagrams of the GSCC controller

where: $K = -v_d$, v_d: d-axis stator voltage

The GSCC consists of two fast inner d-q-axis current control loops which control the current through the filter, and an outer slower control loop that controls the DC-link voltage. Inputs E_{ref} and Q_{ref} are user-defined values of the DC-link voltage and the reactive power exchange with the grid. The measured value E of the DC-link voltage is compared with E_{ref} and the error is reduced to zero by a PI regulator whose output is the reference d-axis filter current i^*_{dl} and its transfer function is given by:

$$F_1(s) = 1.95 * (1 + \frac{1}{0.57296s})$$ (9)

The reference q-axis filter current i^*_{ql} is calculated dividing Q_{ref} by K. The measured d-q-axis filter currents i_{dl}, i_{ql} are compared with i^*_{dl} and i^*_{ql} respectively and the errors are reduced to zero by a PI regulator whose transfer function is given by:

$$F(s) = 0.0973 * (1 + \frac{1}{0.008836s})$$ (10)

The Internal Model Control (IMC) method for designing the PI controllers is chosen by the authors [9]. Inputs ω_e and v_q are the stator angular frequency and q-axis stator voltage. The outputs of the current controllers are the d-q-axis converter terminal voltages v^*_{dl} and v^*_{ql} respectively. From these, and applying the inverse Park's transformation, three power frequency sinusoidal voltage references are obtained, as required by PWM technique.

The GSCC controller is implemented in TACS in the following way: a) the E_{ref} and Q_{ref} come from the user defined scenarios b) the filter currents and stator voltages in phase

quantities are measured and passed to TACS by Type-90 and Type-91 sources. The Park's transformation is written in TACS and then dq0 values are derived c) the DC-link voltage is measured and passed into TACS by Type-90 source d) the inverse Park's transformation is also written in TACS e) the PI transfer functions are represented by S-blocks.

IV. POWER CONTROLLER

The wind turbine control strategy consists of four operation zones based on four wind speed regions, as shown in Fig. 7 for a 2.4 MW turbine [11],[12].
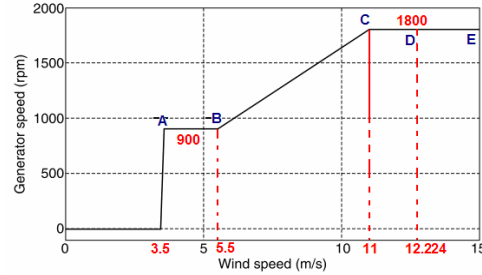

Fig. 7. Operation zones

The Cut-in Speed (minimum wind speed at which the turbine will generate usable power) is 3.5 m/s. The Nominal Wind Speed (the value for which the mechanical power is equal to the rated value) is 12.224 m/s.

Zone AB: has a constant speed operation equal to the minimum wind turbine speed (900 rpm). For each wind sped, λ is calculated, β is set to 0º and C_p is derived. T_{aero} and T_e^{ref}, both referred to the high speed side, are implemented by (4) and (11) in TACS.

$$T_e^{ref} = T_{aero} - D * \omega_r$$ (11)

Zone BC: has a variable speed operation following the maximum power extraction strategy. For each wind speed and generator rotor speed, λ is calculated, β is set to 0º and C_p is derived. T_{aero} referred to the high speed side, is implemented by (4) in TACS. The control strategy consists of taking as the T_e^{ref} the electromagnetic torque related to the maximum power curve, for each generator rotor speed [10],[12]. T_e^{ref} referred to the high speed side, is implemented by (12) in TACS.

$$T_e^{ref} = K_{opt} * (\omega_r)^2 - D * (\omega_r) \quad K_{opt} = \frac{1}{2} * \frac{\rho \pi R^5 C_p^{max}}{\lambda_{opt}^3 * (gearbox\ ratio)^3}$$ (12)

where λ_{opt} corresponds to the maximum value of C_p. When the two torques are equal, the wind turbine reaches the equilibrium point, therefore $\lambda = \lambda_{opt}$ and $C_p = C_p^{max}$.

Zone CD: has a constant speed operation equal to the nominal wind turbine speed ($\omega_t^{nom} = 1800$ rpm) and partial load. The control strategy is the same as zone AB.

Zone DE: has a constant speed operation equal to the nominal wind turbine speed and rated mechanical power (P_{rmp}). When the wind speed is higher than the nominal value, the blades are pitched in order to limit the power extracted from the wind. To do this, the power controller increases β with the purpose of reducing the power coefficient C_p.

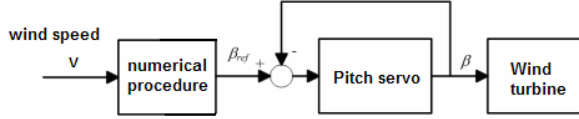Fig. 8 shows the block diagram of the power controller implemented in ATP.

Fig. 8. Power controller

For a given wind speed, λ is first calculated and then the reference pitch angle (β_{ref}) is derived from a non-linear algebraic equation:

$$C_p(\lambda,\beta) = \sum_{i=0}^{4}\sum_{j=0}^{4} \alpha_{ij}\beta^i\lambda^j = \frac{2 * P_{rmp} * \lambda^3}{\rho * \pi * R^5 * (\omega_t^{nom})^3} \quad (13)$$

where the analytical formulation of C_p is described in [4]. A numerical procedure was developed and implemented in TACS using device Type-69, in order to obtain β_{ref}. This value is the input signal of the Pitch Servo Controller [11], whose block diagram is shown in Fig. 9 and represented by S-blocks.
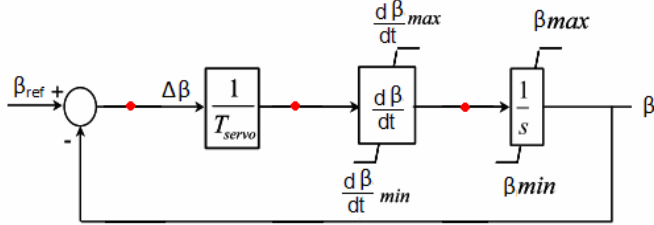

Fig. 9. Pitch Servo Controller

where: T_{servo}=120 ms servo time constant, $(d\beta/dt)_{max}$=8°/s, $(d\beta/dt)_{min}$=-8°/s maximum and minimum pitch rates, β_{max}=30° β_{min}=0° maximum and minimum pitch angle. The output of the pitch controller and λ are used to calculate C_p for each time step and implemented in TACS using device Type-69. Both T_{aero} and T_e^{ref} are implemented in the same way as presented for zone AB.

V. INITIALIZATION PROCEDURE

An initialization procedure of the DFIG type wind turbine model in order to carry out time domain simulations starting from steady state conditions will be presented. The procedure consists of the followings steps for a given wind speed:

1) The wind turbine speed is determined according to the four operation zones. Particularly, for zone BC $\omega_t=\lambda_{opt}*v/R$.

2) T_{aero} and the mechanical power (P_m) are calculated.

3) Induction machine slip (s) and rotor frequency are calculated.

4) Stator power (P_s) and Rotor power (P_r) are calculated as: $P_s=P_m/(1-s)$, $P_r=-sP_s$.

5) An estimate of rotor voltage (V_r) is determined as: $V_r=sV_{ns}/n$, V_{ns} nominal stator voltage, n stator to rotor turn ratio.

6) Fig. 10 shows an electrical network simulated in ATP in order to initialize the RSC. The rotor frequency component of the RSC voltage outputs are represented as three Type-14 sources. V_s and V_r are adjusted in order to fulfill P_s, P_r and power factor at stator terminals. The "Automatic Initialization" of the UM is utilized with the slip derived as in ítem 3). T_{aero} is added to the equivalent network of the UM as a current source

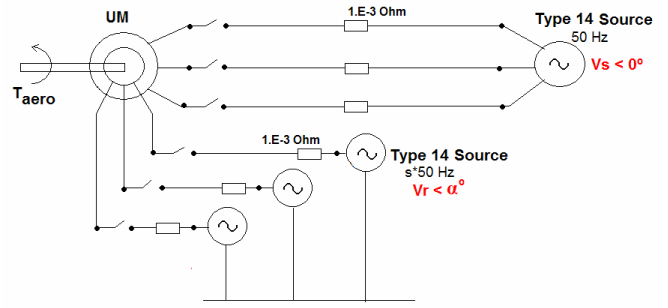Type-14 of 0.00001 Hz for initialization purpose.

Fig. 10. Electrical network for RSC initialization

7) The d-axis angular position for stator magnitudes is $\theta_s=\omega t+\theta_s(0)$. In this case the angle of stator voltage is set to 0° so $\theta_s(0)$=-90°. The d-axis angular position for rotor magnitudes is $\theta_{rot}=(\omega-\omega_r)t+\theta_{rot}(0)$. $\theta_{rot}(0)$ is the initial value of the UM THETAM variable.

8) Once rotor currents, stator and rotor voltages are known from item 6), they will be transformed into d-q-0 quantities. In this way the initial values of v'_{qr}, v'_{dr}, i'_{dr}, i'_{qr}, V_{qs}, λ_{ds} are calculated and then all the initial values of the variables shown in Fig. 5 are determined.

9) The Type-14 sources connected to the rotor, as shown in Fig. 10, are substituted by the RSC for transient simulations. Due to the RSC implementation it is not possible to find a phasor solution during AC steady state. To overcome this problem three Type-14 sources with magnitudes defined as in item 6) are connected to the rotor terminals during AC steady state initialization and removed during transient simulation.

10) Fig. 11 shows an electrical network simulated in ATP in order to initialize the GSC. The power frequency component of the GSC voltage outputs are represented as three Type-14 sources. V_L is adjusted in order to fulfill zero reactive power and near P_r active power exchange with the grid.
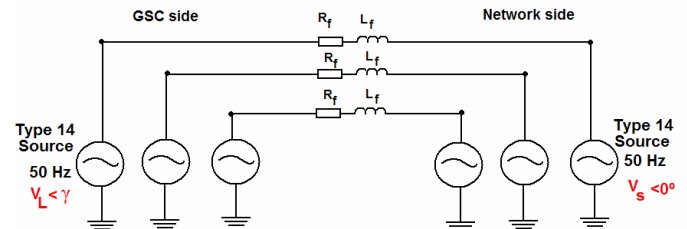

Fig. 11. Electrical network for GSC initialization

11) The d-axis angular position for grid magnitudes is $\theta_g=\omega t+\theta_g(0)$. In this case the angle of stator voltage is set to 0° so $\theta_g(0)$=0°.

12) Once filter currents, stator and converter terminal voltages are known from item 10), they will be transformed into d-q-0 quantities. In this way the initial values of v^*_{dl}, v^*_{ql}, v_q, v_d, i_{dl}, i_{ql}, are calculated and then all the initial values of the variables shown in Fig. 6 are determined.

13) The Type-14 sources connected to the left side of the filter are substituted by the GSC for transient simulations. To overcome the problem presented in item 9) three Type-14 sources with magnitudes defined as in item 10) are connected to the converter terminals during AC steady state initialization and removed during transient simulation.

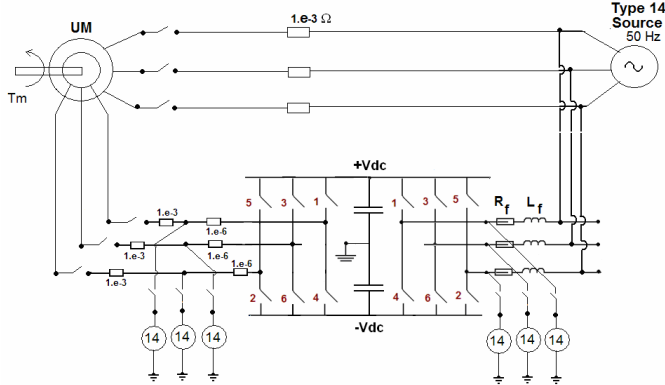Fig. 12 shows the complete model of the DFIG type wind turbine implemented in ATP.

Fig. 12. Complete DFIG model

VI. CASE STUDIES

In order to evaluate the performance of the DFIG type wind turbine model, a 2.4 MW wind turbine has been selected for the case studies. From [12] it is possible to get the basic data: turbine parameters, mechanical system parameters, main characteristics and electrical parameters of the generator. From [13] are selected: DC-link voltage and capacitor values, grid filter parameters and PWM switching frequencies.

A. Scenario with high wind speed - Zone DE

In this scenario the time series shown in Fig. 2 is applied to the DFIG model presented in this paper in order to observe the power controller performance. Fig. 13 shows the time variation of the reference pitch angle β_{ref} and the actual pitch angle β due to power controller action.
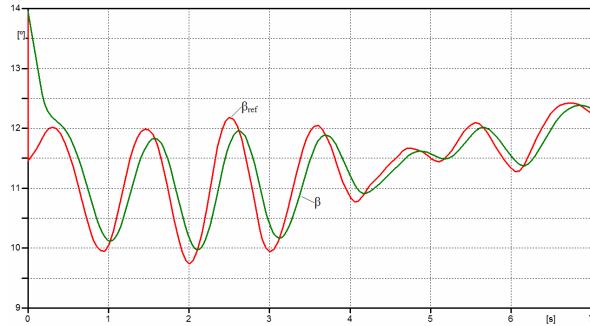

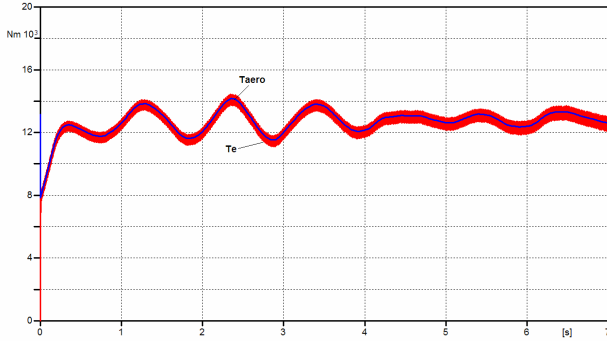Fig. 13. Pitch angles β_{ref} and β

Fig. 14. Aerodynamic (blue) and electromagnetic (red) torques

The pitch angle varies in accordance to wind variation and this is also reflected in the aerodynamic and electromagnetic reference torques, as shown in Fig. 14, in order to limit the active power generated. The sum of stator and rotor active powers (P_{tot}) remains near the 2.4 MW limit, as depicted in Fig. 15.
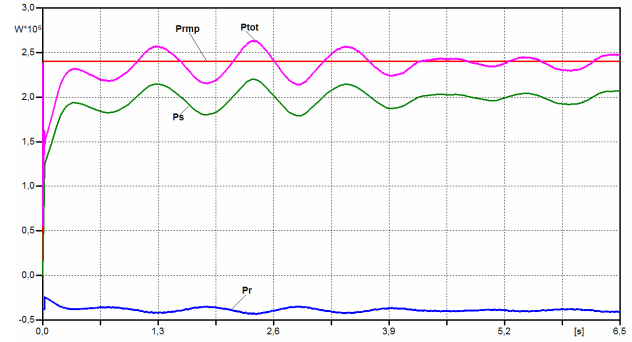

Fig. 15. Stator (P_s), rotor (P_r), nominal (P_{rmp}) and P_{tot} active powers

From these figures it could be observed a good performance of the power controller.

B. Scenario with a three-phase fault - Zone CD

Fig. 16 shows the one-line single diagram of one radial distribution network in the 31.5 kV voltage level, connected to the wind generator. A three-phase fault with a fault resistance is applied at the BUS40 bus bar, at t=0.150 s for 300 ms.
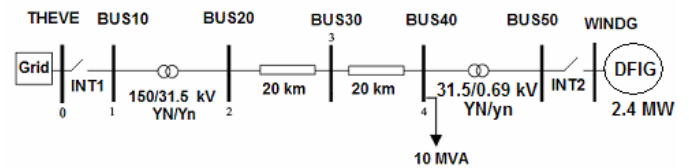

Fig. 16. Radial distribution system

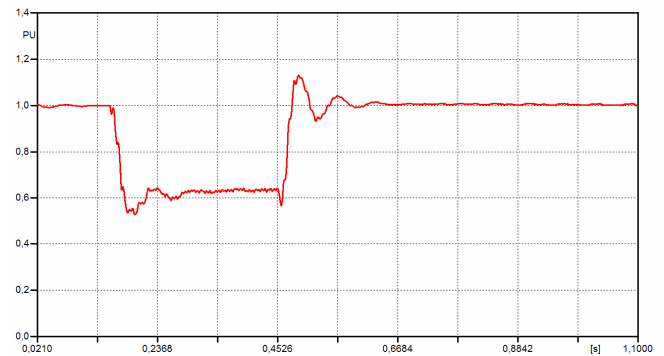As can be seen in Fig. 17 the stator voltage shows a dip of 36.5% during the fault.

Fig. 17. Stator voltage in pu

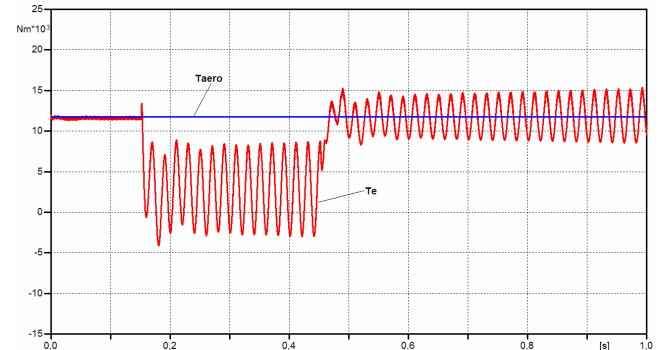The aerodynamic and electromagnetic torques are depicted in Fig. 18.

Fig. 18. Aerodynamic and electromagnetic torques

Due to physical reasons, during the voltage dip period the electromagnetic torque (T_e) presents some oscillations as can be seen in Fig.18. When a voltage dip occurs the stator flux does not change instantaneously, its evolution can be described through an ordinary differential equation. The solution is composed of two terms: homogeneous solution termed as "natural flux" and the particular solution termed as "forced flux". The forced flux amplitude is proportional to the grid voltage and the natural flux is a transient flux caused by the voltage change. The amplitude of the transient flux at the beginning of the dip is higher than during normal operation. This predominant component is seen by the rotor windings as a rotating flux at - ω_r speed (generator rotor angular velocity). Therefore rotor currents present two frequency components mainly, one at slip frequency and the other at ω_r. The oscillations mentioned above are also reflected in Park quantities, so that (5) follows this behavior as shown in Fig.18. A more comprehensive explanation could be found in chapter 6 of [12].

During the fault the stator currents increase, therefore high currents are induced in the rotor windings and hence DC-link current increase. Due to the low voltages at DFIG terminals, the gride side converter can not exchange this extra current to the network. As a result there is a charge accumulation on the capacitor and the DC-link voltage rises as can been observed in Fig. 19. In order to avoid this dangerous DC-link voltage rise a remedial action must be implemented, such as a crowbar.
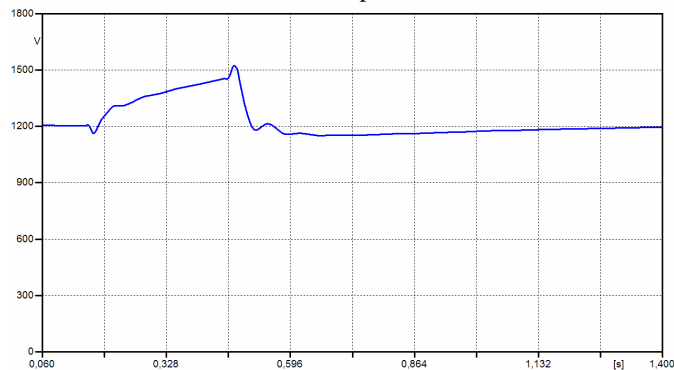

Fig. 19. DC-link voltage

VII. Conclusions

In the present work a comprehensive model of the DFIG type wind turbine is described.

The "Equivalent Wind Speed" model developed by Riso DTU (National Laboratory for Sustainable Energy), Denmark, is chosen as a wind representation in the time domain.

A brief description of the wind turbine basic components together with and explanation of how each of them is simulated in ATP are presented.

The mathematical models of the power converter controllers are presented as complete block diagrams in Laplace domain.

An initialization procedure of the complete DFIG type wind turbine model is delineated.

An explanation of the maximum wind power extraction strategy associated with four wind speed regions is given.

Many simulations have been carried out for the different scenarios corresponding to the four operation zones in order to evaluate the model implementation.

From the results obtained, few of them presented in this work, it can be concluded that:

a) ATP program is an adequate tool for the DFIG type wind turbine simulation.

b) The DFIG type wind turbine model gives satisfactory responses when the "Equivalent Wind Speed" model is considered.

c) The power controller implementation in TACS shows a good performance.

d) The DFIG type wind turbine model developed in ATP could be used to make a comparison with simpler models for conducting other types of studies and for using with other tools.

e) The next step in this investigation is to develop a wind farm model in ATP based on the results and experiences from this work.

VIII. References

[1] P. Rosas, "Dynamic influences of wind power on the power system" Ph.D. dissertation, Dept. Electric Power Engineering, Technical University of Denmark, 2003.

[2] P. Sorensen et alli, "Wind models for simulation of power fluctuations from wind farms" Journal of Wind Engineering and Industrial Aerodynamics, 90(2002), pp. 1381-1402, 2002.

[3] C. Vilar Moreno, "Fluctuaciones de tension producidas por los aerogeneradores de velocidad fija" Ph.D. dissertation, Dept. Ingeniería Eléctrica, Universidad Carlos III de Madrid, 2002.

[4] K. Clark, N.W. Miller, and J.J. Snachez-Gasca, "Modeling of GE Wind Turbines-Generators for Grid Studies", General Electric International, Inc. , Schenectady, NY, Version 4.5, April. 2010.

[5] Alternative Transients Program (ATP)-Rule Book, Canadian / American EMTP User Group, 1987-92.

[6] H. W. Dommel, "EMTP Theory Book", Microtran Power System Analysis Corporation, Vancouver, Canada, 1992.

[7] D. G. Holmes, T. A. Lipo, "Pulse Width Modulation For Power Converters – Principles and Practice", Ed. IEEE PRESS – WILEY INTERSCIENCE, 2003.

[8] J. P. Da Costa, "Contribuicao ao Estudo da Maquina Assíncrona Trifásica Duplamente Alimentada Aplicada a Aerogeradores de Velocidade Variavel" Ms.C. dissertation, PPGEE, Universidade Federal de Santa María, 2006.

[9] L. Harnefors, H. P. Nee, "Robust Current Controlo of AC Machines Using the Internal Model Control Method" IEEE Industry Applications Conference, vol. 1, pp. 303-309, Oct. 1995.

[10] R. Pena, J. C. Clare and J. M. Asher, "Doubly fed induction generator using back-to-back PWM converters and its application to variable-speed wind-energy generation", IEE Proc. Electr. Power Appl. , vol. 143, Nº 3, pp. 231-241, May. 1996.

[11] A. D. Hansen et alli, "Dynamic wind turbine models in power system simulation tool DIgSILENT", Riso-R-1400(EN), Riso National Laboratory, Roskilde, Dec. 2003.

[12] G. Abad et alli, "Doubly Fed Induction Machine – Modeling and Control for Wind Energy Generation", Ed. IEEE PRESS – WILEY, 2011.

[13] R. Ottersten, "Vector Control of a Double-Sided PWM Converter and Induction Machine Drive", Ms.C. dissertation, Dept. of Electric Power Engineering, Univ. Chalmers University of Technology, 2000.